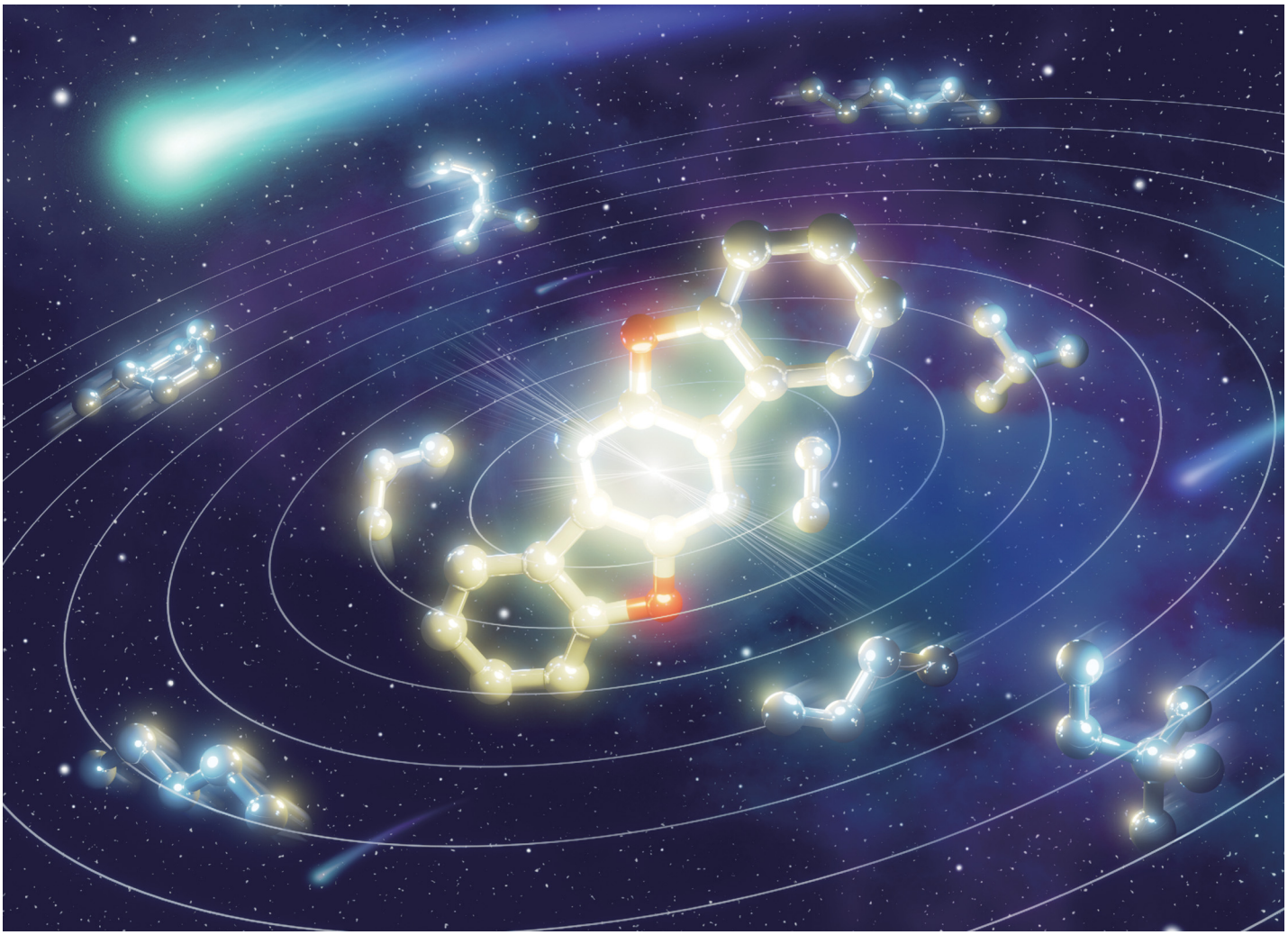

Showing research from Department of Applied Chemistry, Graduate School of Engineering, Osaka University, Japan.

Tunable mechanochromic luminescence of benzofuran-fused pyrazine: effects of alkyl chain length and branching pattern

Introducing various alkyl chains to bisbenzofuropyrazines enables control of both the on/off switching of mechanochromic luminescence and self-recovery rates. This will guide rational design of additional mechanochromic luminescent materials.

As featured in:

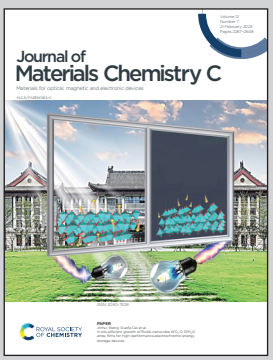

See Koji Hirano, Norimitsu Tohnai *et al.*, *J. Mater. Chem. C*, 2024, **12**, 2370.

ROYAL SOCIETY OF CHEMISTRY

rsc.li/materials-c

Registered charity number: 207890

Journal of Materials Chemistry C

ROYAL SOCIETY OF CHEMISTRY

PAPER

View Article Online
View Journal | View Issue

Cite this: J. Mater. Chem. C, 2024, 12, 2370

Tunable mechanochromic luminescence of benzofuran-fused pyrazine: effects of alkyl chain length and branching pattern†

Shotaro Nakamura,[a] Kohei Okubo,[a] Yuji Nishii,[a] Koji Hirano,*[ab] Norimitsu Tohnai*[a] and Masahiro Miura[b]

Received 23rd December 2023,
Accepted 26th January 2024

DOI: 10.1039/d3tc04748b

rsc.li/materials-c

A series of bis(benzofuro)[2,3-*b*:2′,3′-*e*]pyrazines (**BBFPz**) with various alkyl chains of different length have been synthesized, and the effects of chain length on their mechanochromic luminescent properties were investigated. Some derivatives gave two polymorphs depending on the recrystallization conditions. Although the luminescent properties of the derivatives were almost the same in the solution state, distinct luminescence depending on their alkyl chains was observed in the crystalline state. The obtained crystals could be categorized into four packing motifs (**Type A–D**) with unique mechanochromic luminescent properties. **Type D** crystals with linear alkyl groups did not show mechanochromic luminescent characters. The luminescent color of **Linear-Me** slightly and reversibly changed upon grinding. **Linear-Et** (Form 1) and **Linear-*s*Bu**, which belong to **Type B** and **C**, respectively, exhibited mechanochromic luminescent properties with rapid self-recovery character. The other crystals showed mechanochromic luminescent properties with relatively slow self-recovery rates. The present work demonstrates a quite limited example of covering both on/off mechanochromic luminescence (MCL) and self-recovery characters with a specific luminophore skeleton by changing the alkyl chains.

Introduction

Mechanochromic luminescent materials, which show a color change in response to external mechanical stimuli, have attracted great interest due to their impressive applications in security printing, memory devices, *etc.*[1–3] The development of such smart stimuli-responsive materials is now one of the hot research topics in the field of material science.[4–6] Mechanochromic luminescent active organic small molecules generally exhibit red-shifted emission upon grinding because of the rapid phase transition from the crystalline state to the amorphous state.[7–12] Their original crystalline packing structures are usually recovered by heating or solvent vapor fuming. Some compounds are reported to undergo such recovery processes even by just standing under ambient conditions, which is called ''self-recovery'' character.[13–17] Since a number of mechanochromic luminescent active compounds have been reported over the past two decades, considerable efforts have recently been devoted to elucidating the correlation between molecular/packing structures and their optical properties.[18–20]

The concept of side chain engineering has been recognized as a promising method for controlling physical and optical properties of functional materials.[21–28] Alkyl side chains introduced to the periphery of the core luminophore scaffold significantly change their packing structures. Besides, alkyl groups may improve the solubility of the rigid molecules, which is quite beneficial to allow low-energy and high-volume production as well as wet processes for device fabrication.[29–31] The first example of the alkyl length effect on the mechanochromic luminescent properties was reported by Weder and coworkers in 2008 for oligo(*p*-phenylene vinylene) derivatives.[32] They found that the introduction of long alkoxy groups to the skeleton induced mechanochromic luminescence (MCL). In 2011, Fraser found that a series of difluoroboron diketonates with different alkoxy chain lengths could control the emission shifts, and the recovery time after grinding increased with the elongation of the chain length (Scheme 1).[33] Thomas designed and synthesized dialkylamine-substituted phenylene-ethynylene conjugation systems, and found that alkyl-chain length affected on/off switching of MCL.[34] Afterward, Zhang and Tang investigated the alkyl chain effect on the self-recovery behavior of Au(I) isocyanide complexes.[35] In contrast to Fraser's report, longer alkyl chains could accelerate the self-recovery speed. There are additional examples of side chain engineering for controlling on/off switching of MCL or the self-recovery rate.[36–50]

[a] Department of Applied Chemistry, Graduate School of Engineering, Osaka University, Suita, Osaka, Japan
[b] Innovative Catalysis Science Division, Institute for Open and Transdisciplinary Research Initiatives (ICS-OTRI), Osaka University, Suita, Osaka, Japan

† Electronic supplementary information (ESI) available: Experimental methods, synthetic methods, NMR spectra, HRMS, photophysical data, DSC data, PXRD data, and crystallographic tables. CCDC 2305891–2305902. For ESI and crystallographic data in CIF or other electronic format see DOI: https://doi.org/10.1039/d3tc04748b

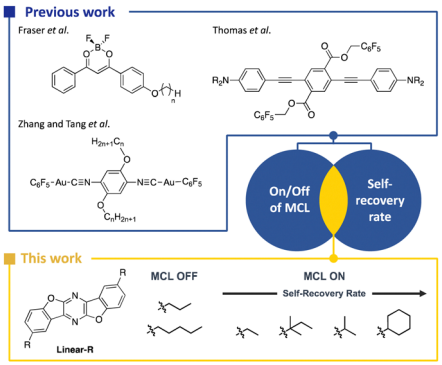

Scheme 1 Organic mechanochromic luminescent materials with various alkyl chains.

Recently, we have synthesized several bis(benzofuro)[2,3-*b*:2′,3′-*e*]pyrazine (BBFPz) derivatives (Fig. 1, **Linear-R**).[51] **Linear-H** (R = H) did not have mechanochromic luminescent properties because of its high planarity and rigid structure. On the other hand, *tert*-butyl substituted **Linear-*t*Bu** (R = *t*Bu) formed two different crystal polymorphs and exhibited self-recovering mechanochromic luminescent properties. Moreover, their bent-type isomers, bis(benzofuro)[2,3-*b*:3′,2′-*e*]pyrazines (**Bent-R**), were also synthesized, and parent unsubstituted bis(benzofuro)[2,3-*b*:3′,2′-*e*]pyrazine (**Bent-H**: R = H) was found to be a good phosphorescent emitter in a dispersed state.[52,53]

In this paper, we report detailed physical and optical properties of a series of newly synthesized alkyl-substituted bis(benzofuro)[2,3-*b*:2′,3′-*e*]pyrazines (**Linear-R**). Some compounds formed crystalline polymorphs under different recrystallization conditions. The obtained crystals could be categorized into four packing motifs with unique mechanochromic luminescent characters. Almost all reported examples of alkyl-chain-controlled mechanochromic luminescent active compounds have flexible and free-rotating single bonds within their core skeletons.[54–56] In sharp contrast, **Linear-R** has a rigid and planar heterocycle luminophore, but the alkyl substituents control the stacking structure to make it sensitive to external stimuli. As a result, the present work demonstrates a quite limited example of covering both on/off switching of MCL and self-recovery characters with a specific luminophore skeleton.

Results and discussion

Synthesis

The synthetic route to the bisbenzofuropyrazine derivatives is shown in Scheme 2. Two-fold nucleophilic substitution of

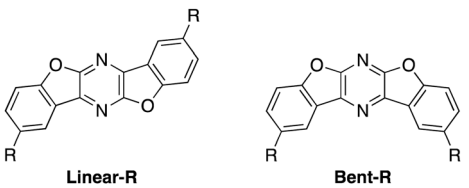

Fig. 1 Structures of linear- and bent-type bisbenzofuropyrazines.

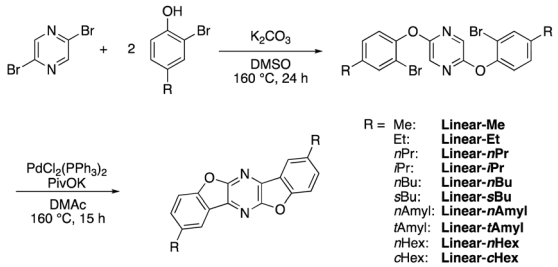

Scheme 2 Synthetic routes to linear-type bisbenzofuropyrazines.

2,5-dibromopyrazine with *o*-bromophenols in basic DMSO solution gave the corresponding 2,5-diphenoxypyrazines, which were then subjected to intramolecular direct arylation conditions using a $PdCl_2(PPh_3)_2$ catalyst to afford the target alkyl-substituted bisbenzofuropyrazines (**Linear-R**).

Optical properties (solution)

Photophysical properties of **Linear-R** were next examined by UV/Vis absorption and photoluminescence (PL) spectroscopy in diluted $CHCl_3$ solutions. All compounds exhibited two characteristic absorption bands with absorption maxima around 260 nm and 380 nm, and emitted blue-violet fluorescence with relatively high luminescence quantum yields (Φ_{FL}) of 0.55–0.93 (Table 1). As a representative example, the absorption and fluorescence spectra of **Linear-Me** are shown in Fig. 2. The photophysical properties of **Linear-R** in the dispersed solution state were less dependent on the alkyl groups.

Crystallization

The synthesized **Linear-R** was reasonably soluble in organic solvents and readily recrystallized, whereas the previously reported **Linear-H** was almost insoluble.[51] **Linear-Et** and **Linear-*c*Hex** crystallized as two polymorphs (Forms 1 and 2) depending on the recrystallization conditions, whereas the other eight compounds did not give polymorphs even after many trials with various solvent/temperature combinations. **Linear-Et** afforded colorless prismatic crystals by slow evaporation from a $CHCl_3$ solution (Form 1) and colorless needle-like crystals by evaporation from a THF solution (Form 2). Variable temperature powder X-ray diffraction (VT-PXRD) measurements revealed that the **Linear-Et** (Form 2) underwent a phase transition to Form 1 around 140 °C, whereas Form 1 exhibited no transition below its melting point (Fig. S1,

Table 1 Summary of absorption and emission spectra

Compound (**Linear-**)	λ_{Abs} (nm)	ε_{max} (10^4 M^{-1} cm^{-1})	λ_{Fl} (nm)	Φ_{Fl} (–)
Me	379	5.25	405	0.85
Et	379	4.76	406	0.77
***n*Pr**	379	3.97	406	0.72
***i*Pr**	379	4.44	407	0.87
***n*Bu**	379	3.99	406	0.81
***s*Bu**	379	5.92	407	0.85
***n*Amyl**	380	4.56	407	0.82
***t*Amyl**	380	5.86	408	0.89
***n*Hex**	380	3.49	406	0.76
***c*Hex**	380	4.35	408	0.55

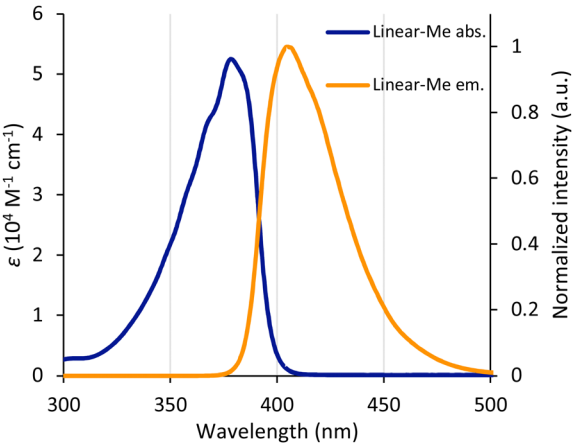

Fig. 2 Absorption and emission spectra of **Linear-Me** in $CHCl_3$ solution. The concentration was maintained at 1×10^{-5} M.

ESI†). This indicates that Form 1 is thermodynamically more stable than Form 2, but the difference in packing stability between Form 1 and Form 2 might be small because DSC measurements of both forms did not show clear peaks around the transition temperature (Fig. S2, ESI†). **Linear-*c*Hex** crystallized as colorless needles by slow evaporation from the CH_2Cl_2 solution (Form 1) and as colorless blocks by slow evaporation from the EtOAc solution (Form 2). VT-PXRD measurements revealed that Form 2 underwent the first phase transition to Form 1 around 190 °C and the second transition occurred just below the melting point (Fig. S1, ESI†). However, similar to **Linear-Et**, DSC measurements of **Linear-*c*Hex** exhibited no clear signal around the transition temperatures (Fig. S2, ESI†).

Crystal structures

The packing arrangements of the **Linear-R** compounds were evaluated by single crystal X-ray crystallographic analyses. All crystal structures showed a face-to-face slipped columnar structure and can be categorized into four packing motifs (**Type A–D**) according to the orientation of the alkyl substituents (Fig. 3 and 4). The classification was based on the mechanochromic luminescent properties, which were consistent with the orientation of the alkyl chains rather than the orientation of the aromatic scaffolds.

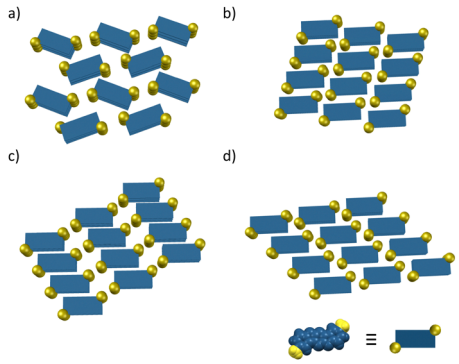

Fig. 3 Stylized models of molecular packing along the columnar structure in the crystalline state: (a) **Type A**, (b) **Type B**, (c) **Type C**, and (d) **Type D**.

Linear-*t*Amyl belongs to the **Type A** group (Fig. 3a and 4). The longest slippage distance of 5.59 Å was observed probably because the sterically demanding *tert*-amyl substituents interrupted face-to-face stacking of the aromatic moieties. **Linear-Me**, **Linear-Et** (Form 1), **Linear-*i*Pr**, and **Linear-*c*Hex** (Form 1) belong to the **Type B** group (Fig. 3b and 4). Here, BBFPz skeletons form intercolumnar contact at the short molecular axis, and the alkyl groups occupy spaces between the π scaffolds along the long axis. The slippage distances were relatively short ranging from 3.19 to 3.30 Å, except for **Linear-Me** crystals (5.12 Å). Because the **Linear-Me** crystal has compact methyl groups compared to the other crystals, relatively weak dispersion energy gave large slippage distance. **Linear-*s*Bu** and **Linear-*c*Hex** (Form 2) belong to the **Type C** group (Fig. 3c and 4), where BBFPz skeletons form intercolumnar contact at the long molecular axis. The alkyl groups were in contact at the short molecular axis. These crystals gave short π–π stacking distances (3.40 Å and 3.33 Å), whereas the bulky alkyl groups prevented further approach towards the mother skeleton to give a slightly larger slippage distance (3.79 Å and 4.06 Å). **Linear-Et** (Form 2), **Linear-*n*Pr**, **Linear-*n*Bu**, **Linear-*n*Amyl**, and **Linear-*n*Hex** belong to the **Type D** packing motif (Fig. 3d and 4). BBFPz skeletons form intercolumnar contact at the long molecular axis, and the alkyl substituents form zipper-like layer structures. The short stacking distance (3.36–3.43 Å) and relatively small slippage distances (3.16–3.29 Å) would reflect the strong π–π interaction within these crystals.

Optical properties (crystal)

The photophysical properties of **Linear-R** in the crystalline state were found to be different from those in solution (Fig. 5 and Table 2). **Linear-*t*Amyl** (**Type A**) exhibited strong blue emission with the emission maximum wavelength (λ_{em_max}) at 438 nm (Fig. 5i). The insertion of bulky *tert*-amyl substituents among the columnar structures prevented the mother skeletons from strong contact, which gave monomeric blue emission. The fluorescence lifetime of 2.86 ns was also indicative of monomeric emission. The quantum efficiency of the crystal was 0.60. The photophysical properties of **Type B** crystals depend on their alkyl substituents. The luminescence spectra of **Linear-Me** and **Linear-*c*Hex** (Form 1) crystals were slightly red-shifted to 448 and 443 nm, respectively, compared with the crystal of **Linear-*t*Amyl** (Fig. 5a and k). The fluorescence lifetimes of the **Linear-Me** and **Linear-*c*Hex** (Form 1) crystals were 2.68 and 10.4 ns, respectively. Additionally, the excitation spectra of the crystals were similar to that of **Linear-*t*Amyl**, indicating that luminescence from **Linear-Me** is monomeric emission and that from **Linear-*c*Hex** (Form 1) is excimer emission.[57–61] **Linear-Et** (Form 1) and **Linear-*i*Pr** showed more red-shifted light-blue emission with the emission maximum wavelength (λ_{em_max}) at 467 and 468 nm with a lifetime (τ_{em}) of 8.51 and 12.6 ns, respectively (Fig. 5b and e). Additionally, the excitation spectra of these crystals were red-shifted compared to that of monomerically emissive **Linear-*t*Amyl**. The observed red-shifted emission and excitation spectra

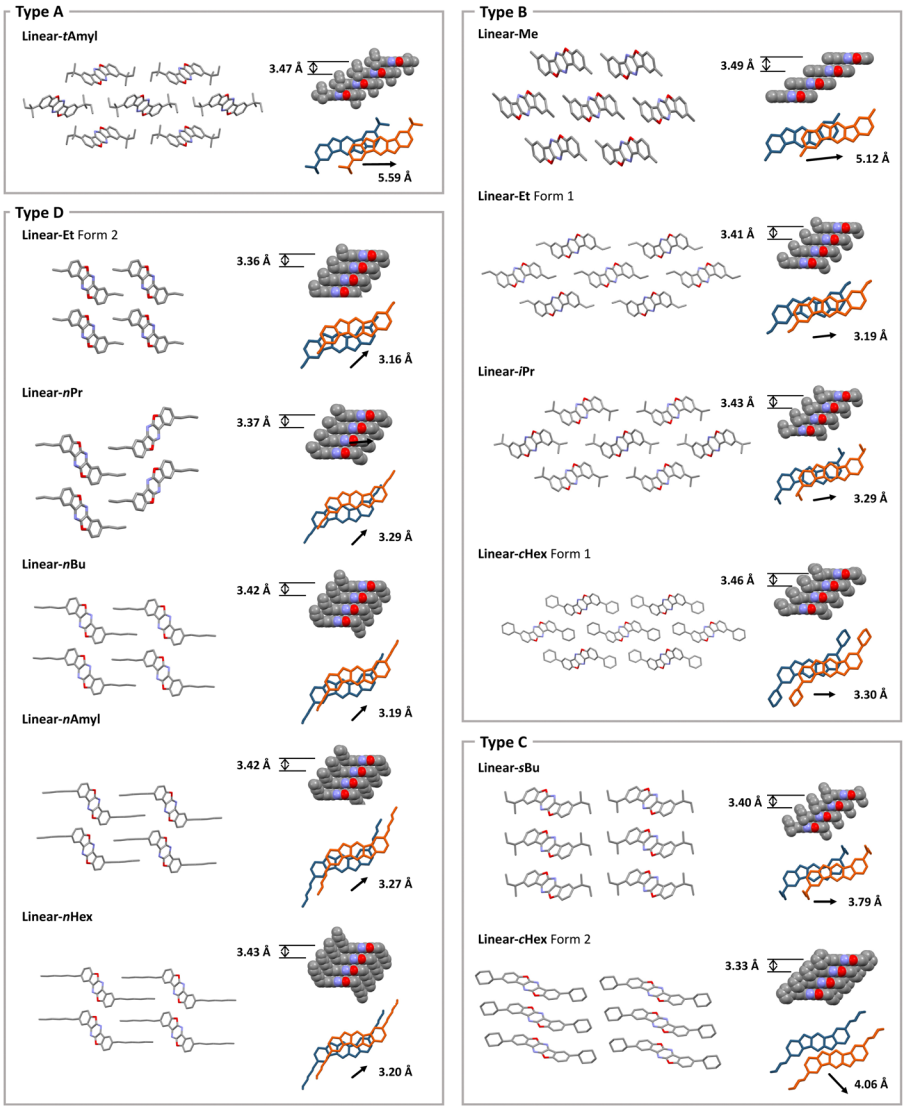

Fig. 4 Categorized crystal structures. Hydrogen atoms are omitted for clarity. The double-headed arrows denote the interplanar distance between the mother skeletons in the columnar structure. The single-headed arrows denote the slippage distance of two adjacent mother skeletons in the columnar structure. Grey: carbon; red: oxygen; purple: nitrogen.

may be caused by strong ground-state interaction due to the close packing structure. The quantum efficiencies of **Linear-Me**, **Linear-Et** (Form 1), **Linear-*i*Pr**, and **Linear-*c*Hex** (Form 1) were 0.28, 0.41, 0.21, and 0.52, respectively. These results indicate that π–π interaction among the luminophores decreased the luminescence.[62] Introducing alkyl groups changed the mode of π–π stacking and tuned the luminescent properties. The photophysical properties of **Type C** crystals were highly dependent on the alkyl side chain. The fluorescence spectrum of the **Linear-*c*Hex** (Form 2) crystals was sharp and slightly red-shifted (λ_{em_max} = 442 nm, τ_{em} = 12.0 ns; Fig. 5l). Its excitation spectra were almost the same as that of **Linear-*t*Amyl**, indicating that excimer emission occurs. The **Linear-*c*Hex** (Form 2) crystals had a close stacking distance, but the mother skeletons were sufficiently separated from each other by bulky cyclohexyl substituents. Thus, its emission was originated not from a ground-state dimer but from an excimer. On the other hand, the crystals of **Linear-*s*Bu** showed more red-shifted and broadened light-blue emission (λ_{em_max} = 462 nm, τ_{em} = 26.2 ns) (Fig. 5g). The quantum efficiencies of **Linear-*s*Bu** and **Linear-*c*Hex** (Form 2) were 0.47 and 0.31, respectively. Crystals of **Type D** (**Linear-Et** Form 2, **Linear-*n*Pr**, **Linear-*n*Bu**, **Linear-*n*Amyl**, **Linear-*n*Hex**) showed similar emission spectra, which were broadened and red-shifted (λ_{em_max}: 469–480 nm, τ_{em} = 12.1–23.0 ns) (Fig. 5c, d, f, h and j). The quantum efficiencies of these crystals ranged from 0.29 to 0.67. In the **Type B** and **Type D** crystals, the fluorescence quantum yields were relatively high as the free volumes in their unit cell decreased (Fig. S3 and Table S1, ESI†). This is probably because the small free volumes minimize molecular vibration to suppress nonradiative decay.[63,64] Apparently, the introduction of various kinds of alkyl substituents to the benzofuropyrazine mother skeleton is a quite important method to control polymorph and luminescence properties.

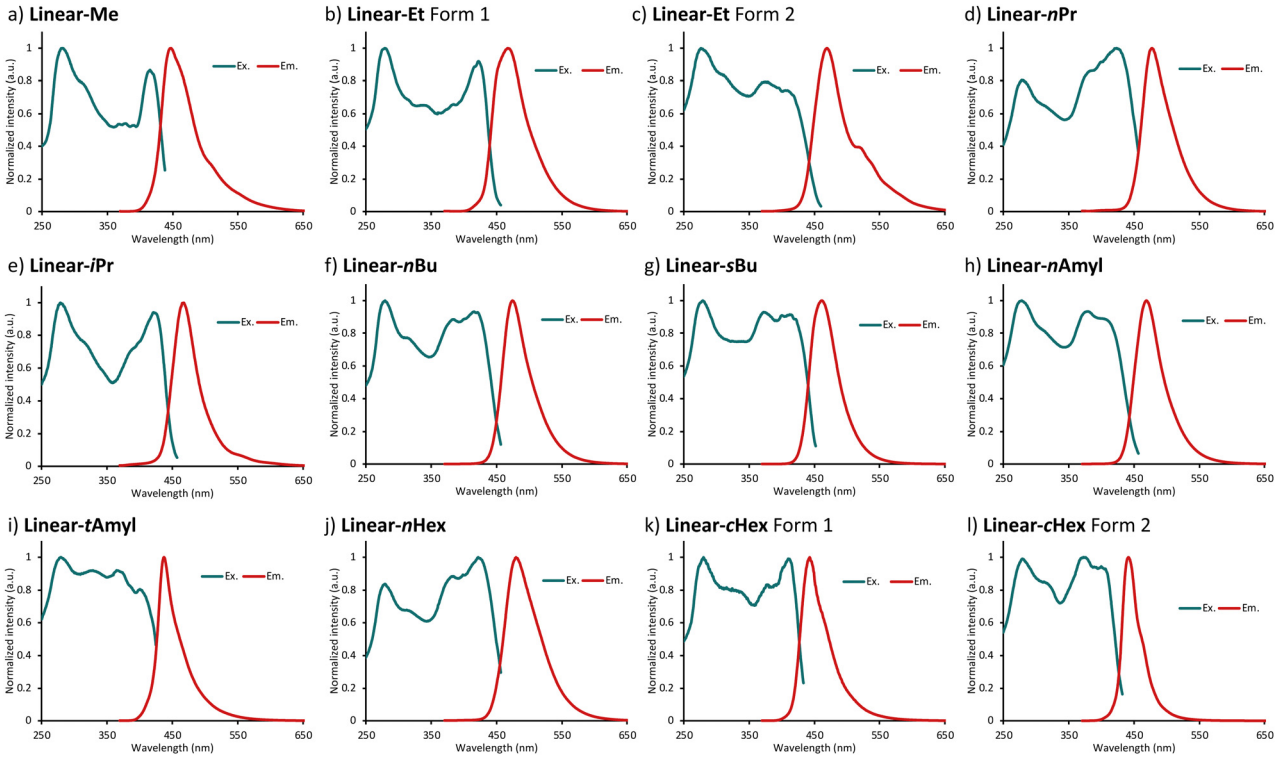

Fig. 5 Excitation and emission spectra of formed crystals. (a) **Linear-Me**, (b) **Linear-Et** Form 1, (c) **Linear-Et** Form 2, (d) **Linear-*n*Pr**, (e) **Linear-*i*Pr**, (f) **Linear-*n*Bu**, (g) **Linear-*s*Bu**, (h) **Linear-*n*Amyl**, (i) **Linear-*t*Amyl**, (j) **Linear-*n*Hex**, (k) **Linear-*c*Hex** Form 1, (l) **Linear-*c*Hex** Form 2.

Mechanochromic properties

The crystals of **Linear-R** showed diverse MCL depending on the alkyl substituents and packing structures (Fig. 6 and Table 2). Crystals categorized into the **Type D** packing structure (**Linear-Et** (Form 2), **Linear-*n*Pr**, **Linear-*n*Bu**, **Linear-*n*Amyl**, and **Linear-*n*Hex**) did not show considerable spectral changes upon grinding (Fig. S4, ESI†). On the other hand, for the **Linear-*t*Amyl** crystals, a relatively long-lived green-emissive state was observed after grinding (Fig. 6c). A new fluorescence band emerged around 509 nm, whereas the original peak at 438 nm decreased and slightly blue-shifted (427 nm). We also investigated the IR spectra of **Linear-*i*Pr** as a representative example before and after grinding, but did not identify any clear difference (Fig. S5, ESI†). Thus, the excitation spectra were measured to clarify the changes of interactions. Excitation spectra measured at 509 and 427 nm were identical to each other, indicating that these two emissions were derived from the same excited species. We conducted powder X-ray diffraction (PXRD) analyses for **Linear-*t*Amyl** before/after grinding (Fig. S7, ESI†). Since the characteristic signals almost disappeared after grinding, it is conclusive that the green-emissive state was almost an amorphous structure (Fig. 7a and b). A similar trend was observed in **Linear-*c*Hex** (Forms 1 and 2) although their spectral changes were somewhat smaller compared to those of **Linear-*t*Amyl** (Fig. 6d and e). **Linear-Me** and **Linear-*i*Pr** exhibited much smaller spectral changes (Fig. 6a and b). According

Table 2 Summary of photophysical data of **Linear-R**

Compound (**Linear-**)	λ_{Fl} (nm)	Φ_{Fl} (−)	τ_{Fl}[a] (ns)	$\lambda_{Fl\ (ground)}$ (nm)	$\lambda_{Fl\ (ground\text{-}heat)}$ (nm)	$\lambda_{Fl\ (ground\text{-}fuming)}$ (nm)
Me	448	0.28	3.07	468	469	467
Et Form 1	467	0.41	8.51	445	—	—
Et Form 2	470	0.67	20.1	471	—	—
***n*Pr**	478	0.35	14.5	475	—	—
***i*Pr**	468	0.21	12.6	518	469	467
***n*Bu**	474	0.49	23.0	471	—	—
***s*Bu**	462	0.47	26.2	448	—	—
***n*Amyl**	469	0.44	17.9	472	—	—
***t*Amyl**	438	0.60	2.86	509	421	417
***n*Hex**	480	0.29	12.1	475	—	—
***c*Hex Form 1**	443	0.52	10.4	516	447	435
***c*Hex Form 2**	442	0.31	12.0	516	434	433

[a] Average emission lifetime.

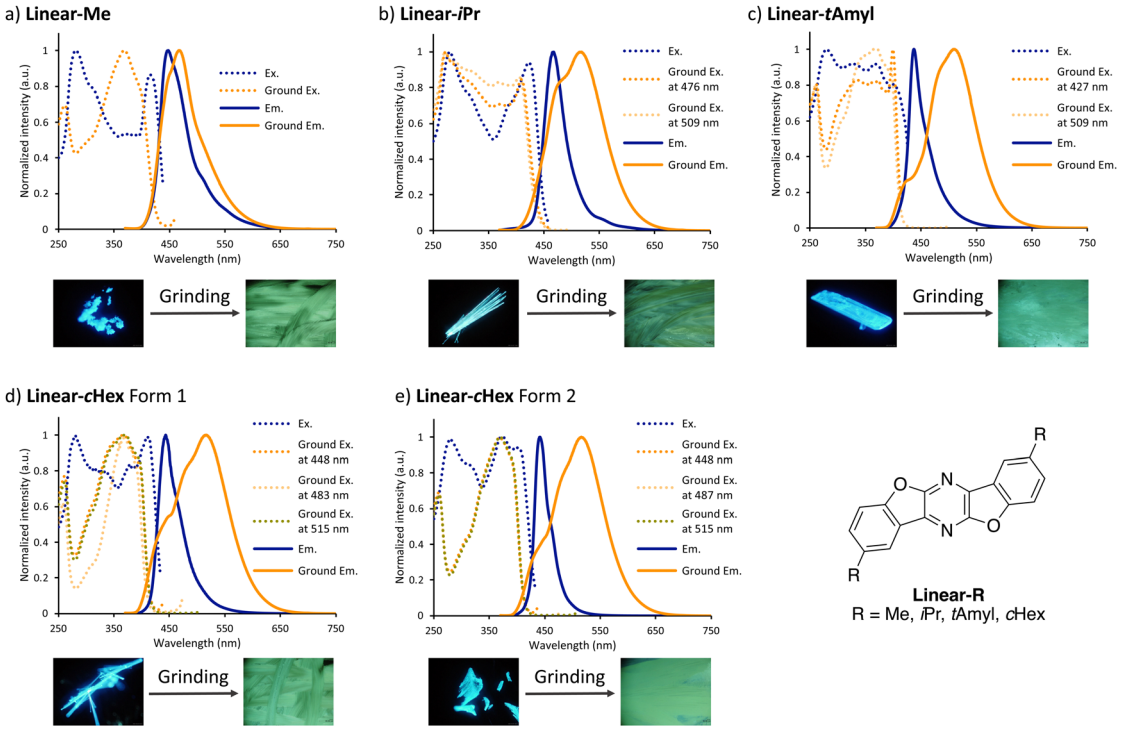

Fig. 6 Excitation spectra (Ex.) and emission spectra (Em.) of the formed crystals and ground powders of (a) **Linear-Me**, (b) **Linear-*i*Pr**, (c) **Linear-*t*Amyl**, (d) **Linear-*c*Hex** Form 1, and (e) **Linear-*c*Hex** Form 2.

to PXRD measurements, **Linear-*c*Hex** (Forms 1 and 2), **Linear-Me**, and **Linear-*i*Pr** were also in amorphous systems after grinding (Fig. S7, ESI†). The fluorescence peak of the **Linear-Et** (Form 1) crystals appeared to be blue shifted upon grinding. However, the self-recovery process (*vide infra*) was too fast to capture red-shifted peaks during grinding (Fig. S4a, S6 and Video 1, ESI†). **Linear-*s*Bu** crystals exhibited a similar behavior to **Linear-Et** (Form 1; Fig. S4 and Video 2, ESI†).

Relationship between MCL and crystal structure

The BBFPz scaffold within **Linear-*t*Amyl** crystals (**Type A**) was surrounded by flexible *tert*-amyl groups with considerably large free volume (Fig. 3a and 4). External mechanical stimuli would effectively disturb the packing structure to form suitable sites for excimer emission. As a result, distinct red-shifted emission was observed after grinding (Fig. 6c). As for **Linear-*c*Hex** crystals (Forms 1 and 2), the BBFPz skeleton shows considerable short intermolecular contact (Fig. 3b, c and 4). This interaction would make these crystals less responsive to external mechanical stimuli, thereby showing smaller changes in their spectral shapes upon grinding (Fig. 6d and e). This mechanism was also supported by calculation of intermolecular potentials in the crystalline state (Fig. S8, ESI†).[65,66] **Linear-Me** and **Linear-*i*Pr** also exhibited MCL but with smaller color changes. Since **Linear-Me** and **Linear-*i*Pr** have sterically much less demanding alkyl groups, their fluorescence spectra did not significantly change after grinding (Fig. 6a and b). A similar trend was observed in our previous work.[51] In contrast, the packing system of **Type D** crystals, **Linear-Et** (Form 2), **Linear-*n*Pr**,

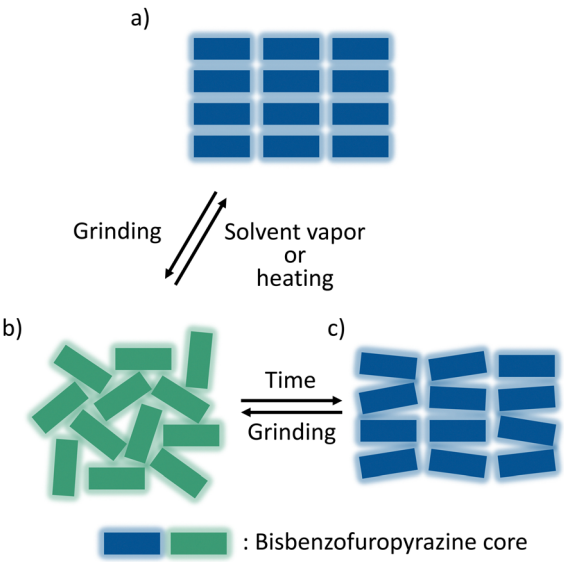

Fig. 7 Illustration of molecular arrangement models after various stimuli. (a) Pristine powder, (b) powder after grinding, low-ordered amorphous, and (c) ground powder after self-recovery.

Linear-*n*Bu, **Linear-*n*Amyl**, and **Linear-*n*Hex**, would be rather rigid because their columnar structures are anchored by the interaction between relatively long linear alkyl substituents, thereby not showing characteristic mechanochromism (Fig. 3d and 4). Theoretical calculations show that the intermolecular interaction energies between stacked molecules increase on

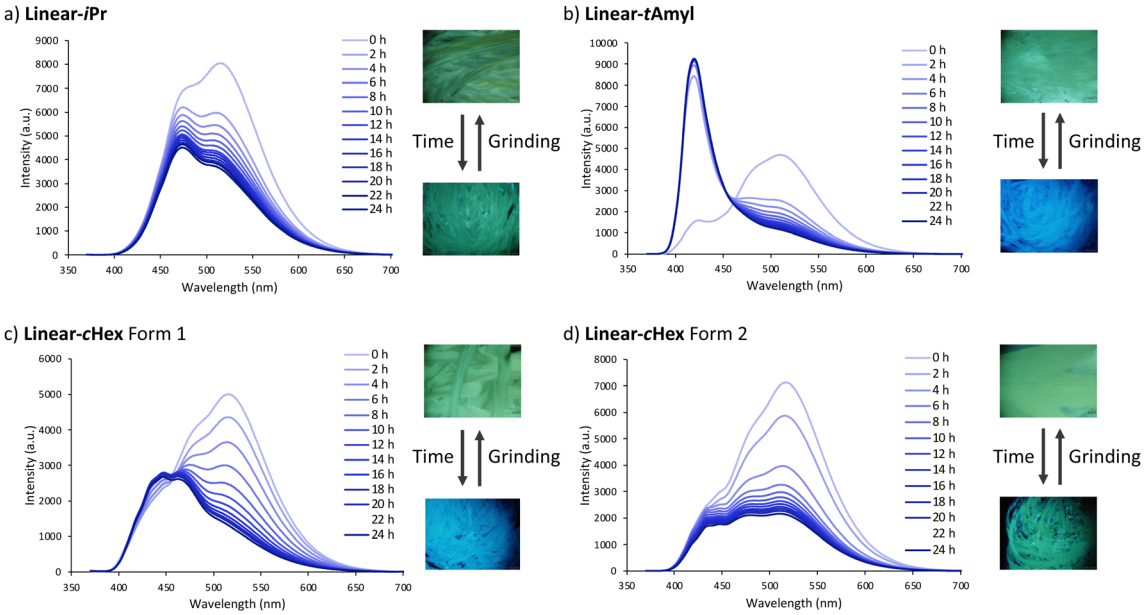

Fig. 8 Change over time of luminescence after mechanical stimuli. (a) **Linear-*i*Pr**, (b) **Linear-*t*Amyl**, (c) Form 1 of **Linear-*c*Hex**, and (d) Form 2 of **Linear-*c*Hex**.

increasing the number of carbons in the alkyl groups, which is also known as the "fastener effect" (Table S2, ESI†).[67]

Self-recovery of fluorescence

We then investigated the self-recovery behavior of the aforementioned five crystals showing MCL: **Linear-Me**, **Linear-*i*Pr**, **Linear-*t*Amyl**, and **Linear-*c*Hex** (Forms 1 and 2). **Linear-Et** (Form 1) and **Linear-*s*Bu** were excluded herein because their recovery processes were too rapid to trace. The rapid self-recovery character might be derived from their rigid packing systems and relatively large free volume around the columnar structures. MCL of **Linear-Me** can be regarded as irreversible since its fluorescence spectrum remained unchanged after 24 h (Fig. S9, ESI†). The other four compounds recovered their original blue color luminescence by just standing under ambient conditions. **Linear-*t*Amyl** showed the most remarkable recovery profile: the monomeric emission at around 410 nm increased, whereas the excimer emission at around 510 nm almost disappeared even over 24 h (Fig. 8b). Interestingly, the PXRD patterns of the ground **Linear-*t*Amyl** did not change after 24 h (Fig. S10, ESI†). We assume that the molecular arrangement of **Linear-*t*Amyl** becomes low-ordered amorphous upon grinding, in which some luminophores are oriented closely to form excimers. It then converts to high-ordered amorphous, where luminophores are isolated from each other by the alkyl spacer (Fig. 7c). **Linear-*i*Pr** and **Linear-*c*Hex** (Forms 1 and 2) also exhibited self-recovery character at room temperature but much slower than **Linear-*t*Amyl** (Fig. 8a, c and d). This is probably due to the smaller size of free volume around the aromatic scaffold within their packing structures to recover the original structure, thus requiring prolonged periods for the completion of recovery (Fig. S3, ESI†). Considering the absence of self-recovery characters in **Linear-R** with relatively compact substituents such as H[51] or Me, and linear alkyl groups, it is suggested that the presence of relatively bulky substituents with branched alkyl chains plays a crucial role in exhibiting self-recovering characters. The overall decrease of emission intensity during the experiments can be attributed to the degradation of these compounds by the excitation light. The recovery process was significantly accelerated by heating or exposure to $CHCl_3$ vapor, and their original blue-emissive states were restored within 1 minute (Fig. S11, ESI†). After heating or fuming the powders with $CHCl_3$ vapor, the PXRD peaks of the sample reappear, which suggests the recovery of the ordered structure (Fig. S12 and S13, ESI†). The PXRD pattern of the recovered states matched well with that of the initial powder, indicating that heating or vapor fuming accelerates the recovery process to the original crystalline state. As mentioned above, this process would be dependent on the nature of the side chains rather than the stress size and direction of mechanical forces. In addition, the luminescence color change of **Linear-*i*Pr**, **Linear-*t*Amyl**, and **Linear-*c*Hex** (Forms 1 and 2) by grinding and $CHCl_3$ fuming could be repeated at least five times (Fig. S14, ESI†).

Conclusions

A series of bis(benzofuro)[2,3-*b*:2′,3′-*e*]pyrazines modified with different alkyl chains (**Linear-R**) were synthesized in this study. The obtained compounds exhibited similar luminescence properties in solution, regardless of the alkyl substituents. However, they showed distinct luminescent properties in the crystalline state. **Linear-Et** and **Linear-*c*Hex** formed two crystalline polymorphs (Forms 1 and 2) under different recrystallization conditions, while other compounds gave a single crystal under any

tested conditions. Their mechanochromic luminescent properties are highly dependent on the alkyl side chains. Derivatives with long linear alkyl chains did not show MCL. On the other hand, other derivatives bearing smaller or branched alkyl groups exhibited MCL. The peaks emerging at longer wavelength in the ground powders stem from excimer emissions. Mechanical force causes a crystalline-to-amorphous transition as shown by PXRD measurement. The ground powder with large free volume around the mother skeleton in the columnar structures showed relatively short recovery times, and the ground powder with small free volume gave relatively long recovery times. Overall, this work demonstrates how the alkyl chains with different length and size affect the mechanochromic luminescent properties in the crystalline state. Additionally, this is a limited example of controlling the on/off switching of MCL and self-recovery rate with the same mother skeleton by changing the alkyl chains. These unique systems could be promising candidates for application as light-emitting devices, and the findings obtained in the present study will guide the rational design of additional mechanochromic luminescent materials.

Author contributions

S. N. performed all experiments. K. O. supported VT-PXRD measurement. K. H., N. T., and M. M supervised the project. Y. N. supported X-ray analysis. S. N., Y. N., K. H., and N. T. prepared the manuscript. All the authors discussed the results and commented on the manuscript.

Conflicts of interest

There are no conflicts to declare.

Acknowledgements

This work was supported by JSPS KAKENHI Grant No. JP 22H02077 (Grant-in-Aid for Scientific Research (B), to K. H.) and JP 17H06092 (Grant-in-Aid for Specially Promoted Research, to M. M.), and by JST FOREST Program, Grant Number JPMJFR211X to K. H. as well as by JST SPRING, Grant Number JPMJSP2138 to S. N.

Notes and references

1 X. Liu, M. Li, M. Liu, Q. Yang and Y. Chen, *Chem. – Eur. J.*, 2018, **24**, 13197–13204.
2 Y. Wang, X. Tan, Y.-M. Zhang, S. Zhu, I. Zhang, B. Yu, K. Wang, B. Yang, M. Li, B. Zou and S. X.-A. Zhang, *J. Am. Chem. Soc.*, 2015, **137**, 931–939.
3 A. Pucci and G. Ruggeri, *J. Mater. Chem.*, 2011, **21**, 8282–8291.
4 F. Nie and D. Yan, *Angew. Chem., Int. Ed.*, 2023, **62**, e202302751.
5 B. Zhou and D. Yan, *Adv. Funct. Mater.*, 2023, **33**, 2300735.
6 Y. Yang, X. Yang, X. Fang, K.-Z. Wang and D. Yan, *Adv. Sci.*, 2018, **5**, 1801187.
7 Z. Chi, X. Zhang, B. Xu, C. Ma, Y. Zhang, S. Liu and J. Xu, *Chem. Soc. Rev.*, 2012, **41**, 3878–3896.
8 Z. Ma, Z. Wang, M. Teng, Z. Xu and X. Jia, *ChemPhysChem*, 2015, **16**, 1811–1828.
9 Y. Sagara, S. Yamane, M. Mitani, C. Weder and T. Kato, *Adv. Mater.*, 2016, **28**, 1073–1095.
10 C. Wang and Z. Li, *Mater. Chem. Front.*, 2017, **1**, 2174–2194.
11 Z. Yang, Z. Chi, Z. Mao, Y. Zhang, S. Liu, J. Zhao, M. P. Aldred and Z. Chi, *Mater. Chem. Front.*, 2018, **2**, 861–890.
12 S. Ito, *Chem. Lett.*, 2021, **50**, 649–660.
13 L. Bu, M. Sun, D. Zhang, W. Liu, Y. Wang, M. Zheng, S. Xue and W. Yang, *J. Mater. Chem. C*, 2013, **1**, 2028–2035.
14 G. R. Krishna, M. S. Kiran, C. L. Fraser, U. Ramamurty and C. M. Reddy, *Adv. Funct. Mater.*, 2013, **23**, 1422–1430.
15 P. S. Hariharan, N. S. Venkataramanan, D. Moon and S. P. Anthony, *J. Phys. Chem. C*, 2015, **119**, 9460–9469.
16 S. Ito, T. Yamada, T. Seki, Y. Yamaguchi and M. Asami, *Chem. – Asian J.*, 2016, **11**, 1963–1970.
17 T. Wang, N. Zhang, K. Zhang, J. Dai, W. Bai and R. Bai, *Chem. Commun.*, 2016, **52**, 9679–9682.
18 Y. Yang, X. Fang, S.-S. Zhao, F. Bai, Z. Zhao, K.-Z. Wang and D. Yan, *Chem. Commun.*, 2020, **56**, 5267–5270.
19 B. Lu, S. Liu and D. Yan, *Chin. Chem. Lett.*, 2019, **30**, 1908–1922.
20 D. Yan and D. G. Evans, *Mater. Horiz.*, 2014, **1**, 46–57.
21 K. O'Hara, C. J. Takacs, S. Liu, F. Cruciani, P. Beaujuge, C. J. Hawker and M. L. Chabinyc, *Macromolecules*, 2019, **52**, 2853–2862.
22 C. J. Zeman and K. S. Schanze, *J. Phys. Chem. A*, 2019, **123**, 3293–3299.
23 P. Schmode, A. Savva, R. Kahl, D. Ohayon, F. Meichsner, O. Dolynchuk, T. Thurn-Albrecht, S. Inai and M. Thelakkat, *ACS Appl. Mater. Interfaces*, 2020, **12**, 13029–13039.
24 Y.-C. Lin, C.-K. Chen, Y.-C. Chiang, C.-C. Hung, M.-C. Fu, S. Inagaki, C.-C. Chueh, T. Higashihara and W.-C. Chen, *ACS Appl. Mater. Interfaces*, 2020, **12**, 33014–33027.
25 Y. Ding, F. Zhao, S. Kin, X. Wang, H. Lu, G. Zhang, K. Cho and L. Qiu, *ACS Appl. Mater. Interfaces*, 2020, **12**, 41832–41841.
26 S.-H. Kang, D. Lee, H. Kim, W. Choi, J. Oh, J. H. Oh and C. Yang, *ACS Appl. Mater. Interfaces*, 2021, **13**, 52840–52849.
27 X. Wang, S. Liu, C. Ren, L. Cao, W. Zhang and T. Wu, *Macromolecules*, 2022, **55**, 6415–6425.
28 K. Perera, W. Wu, L. You, J. F. Elman, Z. Wang, X. Wang, M. Ahmed, Z. Ke and J. Mei, *Macromolecules*, 2023, **56**, 480–489.
29 J.-H. Jou, S. Kumar, D. Tavgeniene, C.-C. An, P.-H. Fang, E. Zaleckas, J. V. Grazulevicius and S. Grigalevicius, *J. Mater. Chem. C*, 2014, **2**, 8707–8714.
30 J. Chen, C. Shi, Q. Fu, F. Zhao, Y. Hu, Y. Feng and D. Ma, *J. Mater. Chem.*, 2012, **22**, 5164–5170.
31 J.-H. Jou, C.-J. Li, S.-M. Shen, S.-J. Peng, Y.-L. Chen, Y.-C. Jou, J. H. Hong, C.-L. Chin, J.-J. Shyue, S.-P. Chen, J.-Y. Li, P.-H. Wang and C.-C. Chen, *J. Mater. Chem. C*, 2013, **1**, 4201–4208.
32 J. Kunzelman, M. Kinami, B. R. Crenshaw, J. D. Protasiewicz and C. Weder, *Adv. Mater.*, 2008, **20**, 119–122.
33 N. D. Nguyen, G. Zhang, J. Lu, A. E. Sherman and C. L. Fraser, *J. Mater. Chem.*, 2011, **21**, 8409–8415.

34 S. A. Sharber, K.-C. Shih, A. Mann, F. Frausto, T. E. Haas, M.-P. Nieh and S. W. Thomas, *Chem. Sci.*, 2018, **9**, 5415–5426.
35 Y. Dong, J. Zhang, A. Li, J. Gong, B. He, S. Xu, J. Yin, S. H. Liu and B. Z. Tang, *J. Mater. Chem. C*, 2020, **8**, 894–899.
36 Y. Wang, W. Liu, L. Bu, J. Li, M. Zheng, D. Zhang, M. Sun, Y. Tao, S. Xue and W. Yang, *J. Mater. Chem. C*, 2013, **1**, 856–862.
37 L. Bu, Y. Li, J. Wang, M. Sun, M. Zheng, W. Liu, S. Xue and W. Yang, *Dyes Pigm.*, 2013, **99**, 833–838.
38 M. Zheng, D. T. Zhang, M. X. Sun, Y. P. Li, T. L. Liu, S. F. Xue and W. J. Yang, *J. Mater. Chem. C*, 2014, **2**, 1913–1920.
39 P. Xue, B. Yao, X. Liu, J. Sun, P. Gong, Z. Zhang, C. Qian, Y. Zheng and R. Lu, *J. Mater. Chem. C*, 2015, **3**, 1018–1025.
40 Y. Liu, Y. Lei, M. Liu, F. Li, H. Xiao, J. Chen, X. Huang, W. Gao, H. Wu and Y. Cheng, *J. Mater. Chem. C*, 2016, **4**, 5970–5980.
41 T. Han, X. Gu, J. W. Y. Lam, A. C. S. Leung, R. T. K. Kwok, T. Han, B. Tong, J. Shi, Y. Dong and B. Z. Tang, *J. Mater. Chem. C*, 2016, **4**, 10430–10434.
42 Z. Chen, Y. Nie and S. H. Liu, *RSC Adv.*, 2016, **6**, 73933–73938.
43 Y. Lei, Y. Zhou, L. Qian, Y. Wang, M. Liu, X. Huang, G. Wu, H. Wu, J. Ding and Y. Cheng, *J. Mater. Chem. C*, 2017, **5**, 5183–5192.
44 L. Qian, Y. Zhou, M. Liu, X. Huang, G. Wu, W. Gao, J. Ding and H. Wu, *RSC Adv.*, 2017, **7**, 42180–42191.
45 S. A. Sharber, K.-C. Shih, A. Mann, F. Frausto, T. E. Haas, M.-P. Nieh and S. W. Thomas, *Chem. Sci.*, 2018, **9**, 5415–5426.
46 M. Ikeya, G. Katada and S. Ito, *Chem. Commun.*, 2019, **55**, 12296–12299.
47 H. Jiang, X.-J. Liu, R.-R. Jia, T.-H. Xu and M. Xia, *RSC Adv.*, 2019, **9**, 30381–30388.
48 H. Gao, P. Xue, J. Peng, L. Zhai, M. Sun, J. Sun and R. Lu, *New J. Chem.*, 2019, **43**, 77–84.
49 Z. Qiu, Z. Yang, W.-C. Chen, L. Xing, S. Hu, S. Ji, Q. Yang, N. Cai, X. Ouyang and Y. Huo, *J. Mater. Chem. C*, 2020, **8**, 4139–4147.
50 H. Hu, Z. Chen and S. Pu, *Tetrahedron Lett.*, 2021, **67**, 152846.
51 S. Nakamura, N. Tohnai, Y. Nishii, T. Hinoue and M. Miura, *ChemPhotoChem*, 2019, **3**, 46–53.
52 S. Nakamura, M. Tsuboi, T. Taniguchi, Y. Nishii, N. Tohnai and M. Miura, *Chem. Lett.*, 2020, **49**, 921–924.
53 M. Tsuboi, S. Nakamura, Y. Nishii, N. Tohnai and M. Miura, *Chem. Lett.*, 2022, **51**, 819–822.
54 Rare examples of MCL with the rigid skeletons: G. Li, Y. Xu, W. Zhuang and Y. Wang, *RSC Adv.*, 2016, **6**, 84787–84793.
55 Rare examples of MCL with the rigid skeletons: T. Kusukawa, S. Shibata, F. Kannen and K. Yoza, *Tetrahedron*, 2022, **111**, 132735.
56 Rare examples of MCL with the rigid skeletons: S. Banerjee, A. Akhuli and M. Sarkar, *Chem. Phys.*, 2023, **565**, 111762.
57 Y. Mizobe, M. Miyata, I. Hisaki, Y. Hasegawa and N. Tohnai, *Org. Lett.*, 2006, **8**, 4295–4298.
58 T. Hinoue, Y. Shigenoi, M. Sugino, Y. Mizobe, I. Hisaki, M. Miyata and N. Tohnai, *Chem. – Eur. J.*, 2012, **18**, 4634–4643.
59 N. Tohnai, M. Sugino, Y. Araki, K. Hatanaka, I. Hisaki and M. Miyata, *Dalton Trans.*, 2013, **42**, 15922–15926.
60 M. Sugino, Y. Araki, K. Hatanaka, I. Hisaki, M. Miyata and N. Tohnai, *Cryst. Growth Des.*, 2013, **13**, 4986–4992.
61 M. Sugino, K. Hatanaka, T. Miyano, I. Hisaki, M. Miyata, A. Sakon, H. Uekusa and N. Tohnai, *Tetrahedron Lett.*, 2014, **55**, 732–736.
62 H. Langhals, T. Potrawa, H. Nöth and G. Linti, *Angew. Chem., Int. Ed. Engl.*, 1989, **28**, 478–480.
63 Y. Mizobe, H. Ito, I. Hisaki, M. Miyata, Y. Hasegawa and N. Tohnai, *Chem. Commun.*, 2006, 2126–2128.
64 M. Sugino, K. HAtanaka, Y. Araki, I. Hisaki, M. Miyata and N. Tohnai, *Chem. – Eur. J.*, 2014, **20**, 3069–3076.
65 A. Gavezzotti, *Acc. Chem. Res.*, 1994, **27**, 309–314.
66 A. Gavezzotti and G. Filippini, *J. Phys. Chem.*, 1994, **98**, 4831–4837.
67 H. Inokuchi, G. Saito, P. Wu, K. Seki, T. B. Tang, T. Mori, K. Imaeda, T. Enoki, Y. Higuchi, K. Inaka and N. Yasuoka, *Chem. Lett.*, 1986, 1263–1266.

